Structure and Interfacial Properties of Spontaneously Adsorbed *n*-Alkanethiolate Monolayers on Evaporated Silver Surfaces

Mary M. Walczak, Chinkap Chung, Scott M. Stole, Cindra A. Widrig, and Marc D. Porter*

Contribution from Ames Laboratory-U.S. Department of Energy and Department of Chemistry, Iowa State University, Ames, Iowa 50011. *Received August 13, 1990*

Abstract: Monolayer films of *n*-alkanethiols ($CH_3(CH_2)_nSH$, n = 3-15, 17) have been spontaneously adsorbed from solution at evaporated Ag films. These monolayers have been characterized with optical ellipsometry, contact angle measurements, and external reflection infrared spectroscopy (IRS). The IRS data indicate that the monolayers with long chains ($n \geq 10$) are predominantly densely packed, crystalline-like structures with all-trans conformational sequences exhibiting average tilts of ~13° from the surface normal. Although less clearly defined, the collective results from all three characterization methods point to a comparably tilted structure for the shorter chain monolayers. The chain tilts at Ag are markedly different from the ~30° tilts for long-chain *n*-alkanethiolate monolayers at Au,[4,10] indicating a difference in the bonding of the sulfur head group at the two metals. For short-chain monolayers, the offset of an odd-even effect by one methylene group at Ag with respect to Au for both the contact angle and IRS data further supports this conclusion. Models that are based on the crystallinity and the electronic properties of the two substrates are presented as possible explanations of the observed structures. These results demonstrate the potential of long-chain thiolate monolayers at Ag as a model molecular system for unraveling the complexities of a variety of interfacial processes.

Introduction

The formation of monolayer films from organosulfur precursors continues to be explored as an approach to construct interfaces with specific structures and properties.[1-14] These films form spontaneously[15] upon immersion of a variety of metal substrates (e.g., Cu,[1,17] Ag,[17-21] Au[2-14,20-25]) into dilute solutions of a thiol-, sulfide-, or disulfide-containing compound. Of these monolayers, those formed at Au from long-chain *n*-alkanethiols[3-6,9,10,20-25] and their substituted analogues[8-14] have been the most extensively studied. The large interest in this particular adsorbate-substrate system stems from the high degree of structural definition afforded by these adsorbates as organic interfaces. As depicted in Scheme I,[21] long-chain thiols oxidatively adsorb at Au to form a highly ordered, densely packed structure with the alkyl chains tilted ~30° from the surface normal.[4,10] Thus, "thiols on Au" provide unique opportunities as model systems for pursuing a variety of fundamental issues pertaining to interfacial processes[26] including wetting[9,12,24] and heterogeneous electron transfer.[3-6,11,13,14]

As part of our interests in this area, we have been surveying the suitability of other metals (e.g., Ag, Cu, Pt, Hg) as substrates for the formation of organosulfur-based monolayers for electrochemical purposes. During this survey, we observed an intriguing difference in the structure of monolayers from *n*-alkanethiols at Ag relative to Au. Particularly striking, in view of the apparent similarities in the chain conformation (predominantly all-trans sequences for a large portion of the alkyl chain) and mode of adsorption (S-H bond cleavage) at the two surfaces,[12,18,19,21] was the difference in the orientation of the alkyl chains. On Ag surfaces, the chains tilt ~13° from the surface normal, whereas their tilt, as previously noted, is ~30° on Au.[4,10]

This paper reports our results of an in-depth examination of the macroscopic details of the structure and interfacial properties of spontaneously adsorbed monolayer films from *n*-alkanethiols ($CH_3(CH_2)_nSH$, n = 3-15, 17) at evaporated Ag films. The details are probed by a variety of techniques, including optical ellipsometry, contact angle measurements, and external reflection infrared spectroscopy (IRS). The data point to a marked difference in the binding of the thiolate head group at Ag in comparison to that at Au, which directs the average tilt of the alkyl chain. We also describe possible models that are based on consideration of the crystallinity and electronic properties of the substrate to explain qualitatively these structural differences. The potential utility of "thiols at Ag" to serve as model systems for fundamental studies of complex interfacial processes will be briefly discussed.

Scheme I

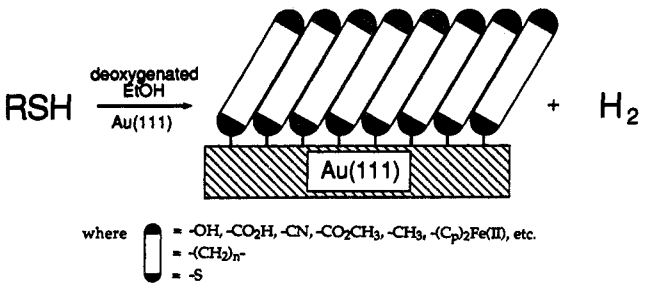

* Author to whom correspondence should be addressed.

(1) (a) Blackman, L. C. F.; Dewar, M. J. S.; Hampson, H. *J. Appl. Chem.* **1957**, *7*, 160-71. (b) Blackman, L. C. F.; Dewar, M. J. S. *J. Chem. Soc.* **1957**, 171-6.
(2) Nuzzo, R. G.; Allara, D. L. *J. Am. Chem. Soc.* **1983**, *105*, 4481-83.
(3) Li, T. T. T.; Weaver, M. J. *J. Am. Chem. Soc.* **1984**, *106*, 6107-8.
(4) Porter, M. D.; Bright, T. B.; Allara, D. L.; Chidsey, C. E. D. *J. Am. Chem. Soc.* **1987**, *109*, 3559-68.
(5) Finklea, H. O.; Avery, S.; Lynch, M.; Furtsch, T. *Langmuir* **1987**, *3*, 409-13.
(6) Sabatani, E.; Rubinstein, I. *J. Phys. Chem.* **1987**, *91*, 6663-9.
(7) Troughton, E. B.; Bain, C. D.; Whitesides, G. M.; Nuzzo, R. G.; Allara, D. L.; Porter, M. D. *Langmuir* **1988**, *4*, 365-85.
(8) Stefely, J.; Markowitz, M. A.; Regen, S. L. *J. Am. Chem. Soc.* **1988**, *110*, 7463-69.
(9) Bain, C. D.; Troughton, E. B.; Tao, Y. T.; Evall, J.; Whitesides, G. M.; Nuzzo, R. G. *J. Am. Chem. Soc.* **1989**, *111*, 321-35.
(10) Nuzzo, R. G.; Dubois, L. H.; Allara, D. L. *J. Am. Chem. Soc.* **1990**, *112*, 558-69.
(11) Chidsey, C. E. D.; Bertozzi, C. R.; Putvinski, T. M.; Mujsce, A. M. *J. Am. Chem. Soc.* **1990**, *112*, 4301-6.
(12) Whitesides, G. M.; Labinis, P. E. *Langmuir* **1990**, *6*, 87-96 and references therein.
(13) Bunding-Lee, K. A. *Langmuir* **1990**, *6*, 709-12.
(14) DeLong, H. C.; Buttry, D. A. *Langmuir* **1990**, *6*, 1319-22.
(15) As exemplified in the recent studies of *n*-alkanoic acid monolayers at oxide covered Al films,[16] *spontaneously adsorbed monolayers* are those which form after a substrate, which has been exposed to the laboratory ambient, is immersed in a surfactant-containing solution.
(16) Allara, D. L.; Nuzzo, R. G. *Langmuir* **1985**, *1*, 45-52.
(17) Labinis, P. E.; Whitesides, G. M.; Allara, D. L.; Tao, Y.; Parikh, A. N.; Nuzzo, R. G. *J. Am. Chem. Soc.* Submitted.
(18) Sandroff, C. J.; Garoff, S.; Leung, K. P. *Chem. Phys. Lett.* **1983**, *96*, 547-51.
(19) Joo, T. H.; Kim, K.; Kim, M. S. *J. Phys. Chem.* **1986**, *90*, 5816-9.
(20) Ulman, A. *J. Mater. Educ.* **1989**, *11*, 205-280.
(21) Widrig, C. A.; Chung, C.; Porter, M. D. *J. Electroanal. Chem.* In press.
(22) Sobocinski, R. L.; Bryant, M. A.; Pemberton, J. E. *J. Am. Chem. Soc.* **1990**, *112*, 6177-83.

0002-7863/91/1513-2370$02.50/0

Experimental Section

Silver Film Preparation. Silver substrates were prepared by the resistive evaporation of 15–20 nm of Cr, followed by 250–300 nm of Ag (99.9%) onto 2-in. diameter polished p-type silicon (111) wafers (Virginia Semiconductors, Inc.). Control experiments with 99.999% Ag gave comparable results. The temperature during the evaporation, measured at the plate supporting the samples, increased to ~50 °C as a result of radiative heating by the evaporation source. The evaporation rates, which were measured with a quartz crystal thickness monitor, were 0.2 and 2.5–3.0 nm/s for Cr and Ag, respectively. The pressure in a cryopumped E360A Edwards Coating System during evaporation was $<9 \times 10^{-5}$ Pa (7×10^{-7} Torr). After the substrates returned to room temperature (~45 min), the evaporator was back-filled with purified N_2, and the substrates were removed.

The surface composition of the evaporated Ag films was examined by Auger electron spectroscopy (AES) in a PHI Auger Multiprobe 600 system. In addition to Ag, the evaporated surfaces contained low levels of sulfur, chlorine, carbon, and oxygen. Sulfur, chlorine, and carbon are attributed to airborne impurities adsorbing upon the removal of the Ag substrates from the evaporator. The presence of oxygen reflects the formation of ca. two to five monolayers of "native" oxide.[27-29] The highly reactive nature of this oxide results in its hydration to a AgOH species in the presence of water at ambient humidities.[30] Using contact angle titrations, we determined that this hydrated surface has an isoelectric point of ~10.4, a value reasonably consistent with that based on the solubility of Ag_2O as a function of pH.[31]

The presence and slow growth of the native oxide at Ag affect sample preparation. Monolayers prepared on substrates which were exposed to the laboratory ambient for different periods of time exhibited slightly different structures, as indicated by IRS. An examination with AES showed that the oxygen content at freshly evaporated Ag films almost doubled for a 2-h exposure to the laboratory ambient. To minimize oxide thickness variations, the exposure of each sample to the laboratory ambient was limited to 10–15 min before being placed in the thiol-containing solution. Further, the data reported here are for different sets of samples prepared from evaporations within the same 24-h period. Trends observed for the long-chain structures were strongly dependent on whether the samples were prepared within the same 24-h time period or over several weeks. The 10–15-min exposure times were necessary for the ellipsometric determination of the complex refractive indices of each of the uncoated Ag samples. Control experiments indicated that monolayers formed on samples that were immersed immediately into the thiol-containing solution upon removal from the evaporator were comparable to those with 10–15-min exposure times.

Monolayer Preparation. *n*-Alkanethiolate monolayers were spontaneously adsorbed onto the evaporated Ag films from dilute (0.1–1.0 mM) solutions in absolute ethanol. Prior to solution preparation, the *n*-alkanethiols were purified either by recrystallization from absolute ethanol or by passage through activity 1 neutral α-alumina. After 12–24 h, the substrates were emersed, rinsed successively with absolute ethanol and hexane, and dried on a photoresist spin coater. These monolayers form quickly since the samples exclude solvent after a few minutes; longer immersion times were used only for convenience.

Ellipsometric Measurements of Film Thickness. The thicknesses of the monolayers were determined by optical ellipsometry in two steps with a computer-interfaced Gaertner Model L-116B ellipsometer at 632.8 nm. Upon removal from the evaporation chamber, the analyzer and polarizer angles for a reflected light beam from each uncoated substrate were measured on at least three different spots. The average complex refractive index for each substrate was then calculated with a two-phase parallel layer model from classical electromagnetic theory.[16,32] After monolayer formation, each sample was again analyzed and the film thickness calculated from a three-phase parallel layer model, using the average complex refractive index of each sample and a real refractive index for the film of 1.45. A value of 1.45, which is representative of the adsorbate precursors,[33] also facilitates comparison with thickness data that have been reported for a variety of other monolayers.[4,5,7,9,12,24] The influence of several possible refinements on the treatment of the ellipsometric data has been recently discussed.[4,9,20]

Contact Angle Measurements. Contact angle measurements with hexadecane and deionized water as probe liquids were measured in air with a Rame-Hart Model 100-00 115 goniometer. Both advancing (θ_a) and receding (θ_r) contact angles were measured. For these measurements, a ~2-μL droplet is formed on the substrate (with the needle of a syringe in the droplet), and the volume of the droplet is slowly increased for θ_a measurements or slowly decreased for θ_r measurements.

Infrared Spectroscopy. Infrared spectra were acquired with a Nicolet 740 FT-IR spectrometer using p-polarized light incident at 80° and a liquid N_2 cooled MCT detector. A home-built sample holder was used to position reproducibly the substrates in the spectrometer.[34] The spectrometer was purged with boil-off from liquid N_2. Spectra were obtained by referencing 1024 sample scans to 1024 background scans at 2-cm^{-1} resolution (zero filled) with Happ–Genzel apodization. All spectra are reported as -log (R/R_0), where R is the reflectivity of the sample and R_0 is the reflectivity of a bare Au reference substrate.

Bare Au references were prepared by immersion in 1:3 H_2O_2 (30%)–H_2SO_4(conc) solution for 5–10 min, and then by rinsing in deionized water and 30% H_2O_2. The references were partially dried on a spin coater and placed immediately into the sample chamber of the spectrometer. After allowing the reference to dry completely in the N_2-purged chamber, the reference spectrum was recorded. This procedure yields a nominally clean surface as verified by the absence of observable C–H stretching bands when referenced to a perdeuterooctadecanethiolate monolayer at Au. *Caution: The H_2O_2/H_2SO_4 solution reacts violently with organic compounds and should be handled with extreme care.*

Reagents. Absolute ethanol (Midwest Grain) and hexane (HPLC grade, Fisher Scientific) were used as received. Prior to use, hexadecane (Aldrich Chemical Co.) was percolated through activity 1 neutral α-alumina until passing the Zisman test.[35] *n*-Alkanethiols ($CH_3(CH_2)_nSH$ with n = 1–9, 11, 13, 15) were acquired from Alfa Products (n = 1), Aldrich (n = 2, 4, 6, 7, 8, 15, 17), Eastman Kodak (n = 3, 5, 9, 11), and Pflatz and Bauer, Inc. (n = 13). *n*-Tridecanethiol and *n*-pentadecanethiol were synthesized from 1-bromotridecane (Aldrich) and 1-bromopentadecane (Aldrich), respectively, with thioacetic acid (Aldrich); the physical characteristics of these compounds were consistent with those previously reported.[9] *n*-Undecanethiol was a gift from Professor George Whitesides (Department of Chemistry, Harvard University). All other chemicals were reagent grade.

Results and Discussion

Elucidation of the structure of organic monolayer films poses a complex problem. To facilitate the presentation of the results of our multitechnique structural studies of *n*-alkanethiolate monolayers at Ag, we have separated the characterization methods into two general classes: those which probe the macroscopic details and those which probe the microscopic details of the films. This paper focuses on the average, or macroscopic, structure of these monolayers. Probes of the microscopic structure include scanning tunneling microscopy, underpotential metal deposition (UPD), and electrochemical reductive desorption, the uses and results of which are the subject of a manuscript in preparation.[36] Of particular relevance to this work are the results of our preliminary Tl(I) UPD studies. From the UPD data, we estimate our evaporated Ag films are ~50% (100) and ~50% (111) and/or (110) facets, results which are consistent with those reported by others at comparably prepared films.[37-39] We also note that the relative amounts of the two faces were somewhat variable (~20%), a result we believe arises from small, uncontrolled differences in our deposition conditions. *This observation is particularly relevant to*

(23) Chidsey, C. E. D.; Liu, G.-Y.; Rowntree, P.; Scoles, G. *J. Chem. Phys.* **1989**, *91*, 4421–3.
(24) Bain, C. D.; Whitesides, G. M. *J. Am. Chem. Soc.* **1989**, *111*, 7164–75.
(25) Strong, L.; Whitesides, G. M. *Langmuir* **1988**, *4*, 546–58.
(26) For additional leading references in this area, see, for example: Swalen, J. D.; Allara, D. L.; Andrade, J. B.; Chandross, E. A.; Garoff, S.; Isrealachvili, J.; McCarthy, T. J.; Murray, R.; Pease, R. F.; Rabolt, J. F.; Wynne, K. J.; Yu, H. *Langmuir* **1987**, *3*, 932–50.
(27) Joyner, R. W.; Roberts, M. W. *Chem. Phys. Lett.* **1979**, *60*, 459–62.
(28) Backx, C.; DeGroot, C. P.; Biloen, P. *Surf. Sci.* **1981**, *104*, 300–17.
(29) Moore, W. M.; Codella, P. J. *J. Phys. Chem.* **1988**, *92*, 4421–26.
(30) Au, C.; Singh-Boparai, S.; Roberts, M. W. *J. Chem. Soc., Faraday Trans. 1* **1983**, *79*, 1779–91.
(31) Parks, G. A.; de Bruyn, P. L. *J. Phys. Chem.* **1962**, *66*, 967–973.
(32) Azzam, R. M.; Bashara, N. M. *Ellipsometry and Polarized Light*; North-Holland Publishing: Amsterdam, 1977.
(33) *Handbook of Chemistry and Physics*; Weast, R. C., Ed.; Chemical Rubber Co.: Boca Raton, FL, 1981.
(34) Stole, S. M.; Porter, M. D. *Appl. Spectrosc.* **1990**, *49*, 1418–20.
(35) Zisman, W. A. *J. Chem. Phys.* **1941**, *9*, 729–41.
(36) Walczak, M. M.; Chung, C.; Alves, C. A.; Widrig, C. A.; Deinhammer, R. S.; Porter, M. D. Manuscript in preparation.
(37) Bagg, J.; Jaeger, H.; Sanders, J. V. *J. Catal.* **1963**, *2*, 449–64.
(38) Gardiner, T. M.; Stiddard, M. H. B. *Thin Solid Films* **1981**, *77*, 335–40.
(39) Jaeger, H.; Mercer, P. D.; Sherwood, R. G. *Surf. Sci.* **1968**, *11*, 265–82.

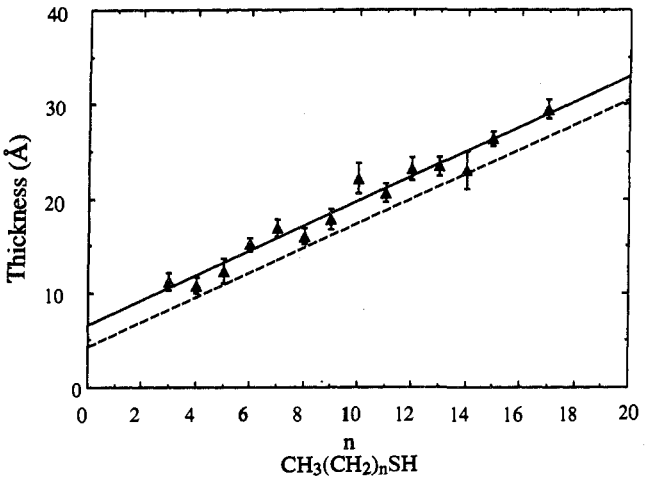

Figure 1. Ellipsometric film thicknesses for monolayers of *n*-alkanethiols ($CH_3(CH_2)_nSH$) adsorbed at Ag. Uncertainties are standard deviations of several measurements on 5–12 different samples. The dashed line represents the thickness of an all-trans alkyl chain extended normal to the surface (see text for details of the calculation).

critical comparisons of results from different laboratories. We will refer to the observations of the microscopic properties of these monolayers throughout the following discussions to support our interpretation of the macroscopic properties.

The experimental techniques used to ascertain the macroscopic properties of these monolayer films include optical ellipsometry, contact angle measurements, and IRS.[16,40] The value of this multitechnique approach is that each measurement probes the structure by a different physical process, providing complementary information. Optical ellipsometry is used to assess the relative thickness of the monolayer films; more subtle details of the structure are addressed by the other techniques. Measurements of the contact angle between a probe liquid and a surface are used for examining wettability as well as for providing inferences about the interfacial composition at the monolayer–probe liquid interface. We used IRS for characterizing the chemical identity and average spatial orientation of the monolayer films.

As we will discuss, the collection of results from these complementary techniques points to a reasonably consistent picture of the average structure for the underlying $-(CH_2)-$ spacer group of our *n*-alkanethiolate monolayers at Ag. Both the wettability and the apparent structure near the chain terminus of these films, however, vary as a function of chain length. These changes are observed at $n = 7$–9, and for the purpose of further discussion, we classify alkyl chains with $n \leq 7$ as short chains and those with $n \geq 10$ as long chains. Though not fully understood, we attribute these variations to two chain length effects: differences in the spatial separation between the air–monolayer and monolayer–substrate interface and/or differing degrees of structural defects. The question of differing degrees of structural disorder is particularly relevant in view of recent low-temperature He diffraction[23] and IRS[41] experiments, which together have implicated the presence of a disordered chain terminus superimposed on an ordered long $-(CH_2)-$ spacer group.

We present first the results obtained with optical ellipsometry and contact angle measurements. A discussion of the IRS data and a description of possible models relevant to the chain packing and head group chemistry follows.

A. Optical Ellipsometric Characterization of Monolayer Film Thickness. The ellipsometric thicknesses of our *n*-alkanethiolate monolayers at Ag are plotted in Figure 1 as a function of *n*, the number of methylene groups in the alkyl chain. These data are reasonably described by the solid line, which is a linear regression fit with a slope of 1.3 Å per CH_2 group and a *y* intercept of 6.6 Å. For comparison to a simple structural model, the dashed line shows calculated thicknesses for *n*-alkanethiolate monolayers consisting of all-trans alkyl chains oriented with their molecular axes normal to the surface. The calculated thicknesses are based on standard bond lengths and bond angles[33,42,43] for alkyl chains. This line has a slope of 1.26 Å per CH_2 group and a *y* intercept equal to 4.58 Å, which corresponds to the length of methanethiolate (CH_3S^-). Comparison to the structural model indicates that the experimental thicknesses are consistent with the formation of a film of one molecular layer. Evidence from IRS confirms this conclusion as well as indicating a lower limit of ~10% for solvent incorporation, as evaluated using perdeuterooctadecanethiolate monolayers formed from various perhydrido solvents. The 10% limit for solvent incorporation represents our estimated detection limit for IRS. We also note that films from both *n*-ethane- and *n*-propanethiol form multilayer structures with thicknesses of several hundred angstroms (not included in Figure 1) and IR absorbances in the C–H stretching region as much as five times greater than those observed for monolayers of longer alkyl chains, a result attributed to an observable corrosive degradation of the Ag films.

The linear increase in the ellipsometric thicknesses in Figure 1 also indicates a consistency in both the conformation and spatial orientation of the alkyl chains for all chain lengths. Further, a comparison of the slopes of the ellipsometric and calculated thicknesses suggests that the alkyl chains are oriented near the surface normal. We believe these thicknesses point to the presence of alkyl chains with all-trans conformational segments, since the presence of disordered structures with many gauche kinks is inconsistent with small chain tilts. This reasoning, in turn, implies that the alkyl chains exist as a densely packed structure. Such an interpretation, however, neither supports or rules out the presence of disordered chain sequences in part of the monolayer structure. Disordered segments of the alkyl chains would result from chains which are conformationally or thermally disordered[23,41] as a result of gauche kinks and/or weak cohesive interchain interactions. In addition, extensively disordered chains most likely exist in regions of structural imperfections of the underlying substrate, viz., grain boundaries.

As noted earlier, our treatment of the ellipsometric data allows a direct comparison to the growing literature on ordered organic films. However, the limitations of our treatment are evident since the experimental thicknesses are consistently ~2 Å larger than those calculated for the model structures in Figure 1. These differences are not fully accounted for by the experimental precision. Similar discrepancies with ellipsometric measurements have also been observed in studies of *n*-alkanethiolate monolayers at Au.[4,9] Three factors stand out as major contributors to these differences: the refractive index of the adsorbed layer, the ubiquitous layer of adsorbed impurities on the "bare" substrate, and the probable change in the refractive index of the substrate following adsorption. As discussed recently, incorporation of these factors through approximations into the physical model we use for the treatment of the ellipsometric data leads to thicknesses of the approximate magnitude to account for the discrepancies in Figure 1.[4,9,20] Irrespective of these quantitative limitations, the ellipsometric thicknesses for our monolayers provide strong evidence for the formation of a film one molecular layer in thickness. Further, through a comparison with model thicknesses, these data point to the presence of a densely packed array of alkyl chains that are composed of all-trans conformational sequences with an average orientation near the surface normal.

B. Contact Angle Measurements of Wetting Characteristics. The results for the advancing contact angles (θ_a) of the *n*-alkanethiolate monolayers are given in Figure 2 for the nonpolar probe liquid hexadecane (HD) and the polar probe liquid water. The uncertainty in these data (sample to sample variation) is ~±2°. For both probe liquids, θ_a's increase with *n* and reach

(40) Allara, D. L.; Nuzzo, R. G. *Langmuir* **1985**, *1*, 52–66.
(41) Nuzzo, R. G.; Korenic, E. M.; Dubois, L. H. *J. Chem. Phys.* **1990**, *93*, 767–73.
(42) Itaya, A.; Van der Auweraer, M.; DeSchryver, F. C. *Langmuir* **1989**, *5*, 1123–26.
(43) Pauling, L. *The Nature of the Chemical Bond*; Cornell University Press: Ithaca, NY, 1960.

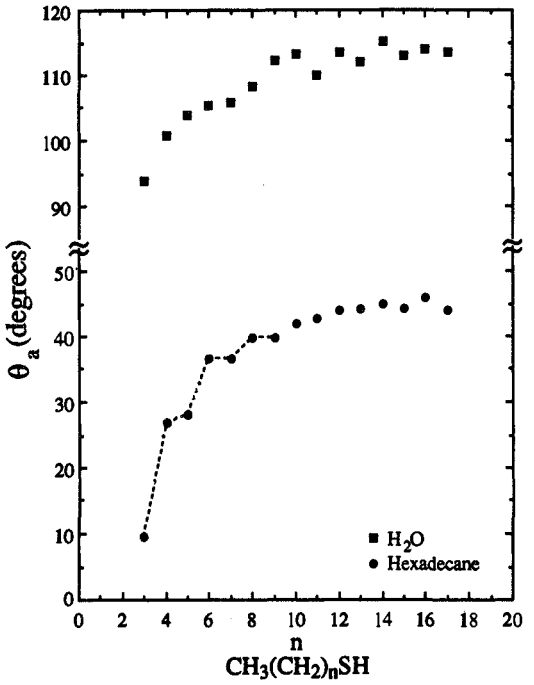

Figure 2. Advancing contact angles of hexadecane (●) and water (■) for monolayers from *n*-alkanethiols ($CH_3(CH_2)_nSH$) at Ag.

limiting values for $n \sim 10$. The limiting θ_a's are ~113° for water and ~44° for HD, and are indicative of an extremely low surface free energy. Such limiting θ_a's are similar to those observed for other well-ordered closely packed alkyl chain monolayers,[9,16,24,44] which argues that our long-chain *n*-alkanethiolate films exhibit a comparably arranged interfacial structure. We also measured θ_r's of 97° for water and 33° for HD for the long-chain structures and markedly lower and less reproducible values for the short-chain structures. As the factors relevant to contact angle hysteresis are not well understood,[45] we will focus only on insights developed from the θ_a data.

For $n < 10$, the θ_a's for water and HD in Figure 2 decrease with chain length. Although we do not fully understand the structural implications, we believe this trend arises from a combination of two sources: an increasing disorder in the structure of the short-chain monolayers and the sensitivity of the probe liquid to the underlying substrate (either through interactions with Ag plasmons or the array of Ag–S dipoles). Others[24] have noted that θ_a's for the above probe liquids are lower at monolayers where disorder has intentionally been introduced, suggesting the presence of disorder in our short-chain structures. Small amounts of disorder have also been predicted by molecular dynamics simulations[46,47] and demonstrated in low-temperature He diffraction studies.[23] The second possible source of the lower θ_a's for the short-chain monolayers is the sensitivity of the probe liquid to the underlying substrate. Recently, we have experimentally verified that the depth sensitivity of wetting to long-range interactions with the underlying head group is inversely proportional to the square of the film thickness.[48] Although difficult to assess their relative contributions, we feel the latter source plays a major role in determining the observed trends.

The θ_a's for HD for the short-chain structures in Figure 2 also exhibit a dependence on whether there are an even or odd number of methylene groups in the alkyl chain. For simplicity, we refer to a chain with an even number of methylene groups as an "even chain" and a chain with an odd number of methylene groups as an "odd chain". Even chain monolayers have θ_a's that are markedly greater than those that are composed of chains with one less methylene group (e.g., θ_a's for $n = 6$ and $n = 5$ are 37° and 28°, respectively). In contrast, θ_a's for odd-chain monolayers are comparable to those for monolayers with one less methylene group (e.g., θ_a's for $n = 5$ and $n = 4$ are 28° and 27°, respectively). Such variations[9,16] suggest the orientation of the terminal methyl group is different for chains with odd and even numbers of methylene groups.[10] Changes in θ_a's with an odd–even variation of chain length may arise from either the resulting microscopic roughness of the interface[9] or a screening of the dispersion forces of the underlying structure by the permanent dipole moment of the methyl group.[48] Both possibilities arise from a difference in the orientation of the terminal methyl group. We do not yet have an explanation as to why this trend "washes out" for the long-chain structures. Possible explanations include the films adopt different structures at long and short chains and/or the long-chain structures are more strongly dependent on subtle conditions of sample preparation which are difficult to isolate and reproduce.

Although further discussion of the structural implications of these data is deferred until the IRS section, it is important to note that the odd–even effect for our short-chain *n*-alkanethiolate monolayers at Ag is offset by one methylene group in comparison to that at Au.[9] *n*-Alkanethiolate monolayers at Au exhibit higher θ_a's for HD for odd-chain monolayers. This offset at Ag in contrast to Au firmly establishes a difference in the structures of the monolayers at the two substrates, which we believe is a direct result of the bonding between the sulfur and metal atoms.

C. Infrared Spectroscopic Characterization of Composition, Molecular Orientation, and Bonding. This section first presents a general description of the IR spectra, and then examines the information provided about the structure and spatial arrangement of the molecules from the CH_2 stretching modes. A discussion of the structural insights derived from the CH_3 stretching modes follows.

(i) General Observations and Mode Assignments. Infrared reflection spectra in the C–H stretching region for our *n*-alkanethiolate monolayers at Ag are shown in Figure 3 for $n = 3$–15, 17. For the long chains (e.g., $n = 17$), five bands are observed. These five bands are ascribed in descending energy to $\nu_a(CH_3,ip)$, $\nu_s(CH_3,FR_1)$, $\nu_a(CH_2)$, $\nu_s(CH_3,FR_2)$, and $\nu_s(CH_2)$. The Fermi-resonance couplet, $\nu_s(CH_3,FR_1)$ and $\nu_s(CH_3,FR_2)$, is designated by the subscripts 1 and 2, which refer to the higher and lower energy components, respectively. These assignments have been discussed in earlier studies of *n*-alkanethiolate monolayers[4,10] and are based on a number of indepth studies of the IR spectroscopy of hydrocarbons.[49,50]

Table I summarizes the peak positions and mode assignments of the spectra in Figure 3 and includes, for comparative purposes, similar data for representative liquid-{$CH_3(CH_2)_5SH$ and $CH_3(CH_2)_{11}SH$} and solid-phase {$CH_3(CH_2)_{17}SH$} *n*-alkanethiols. Orientations of the transition dipoles for the C–H stretching modes in molecular coordinates for an all-trans chain are also listed. The low absorbances of $\nu_s(CH_2)$ and $\nu_a(CH_2)$ for several of the shorter chain monolayers hindered a straightforward determination of their peak positions; overlap with $\nu_s(CH_3,FR_1)$ also complicated the determination of $\nu_a(CH_2)$. More detailed presentations of these data are given in Figures 4 and 5 and in Tables II and III. Data for long-chain *n*-alkanethiolates on Au are provided for comparative purposes in Table III.

(ii) Methylene Modes. We first discuss the spectra of the long-chain monolayers and then analyze these data in terms of chain orientation. An analogous discussion of the short-chain data follows. This section is concluded by examining the molecular orientation of the long-chain structure inferred from the methylene stretching modes. An orientation analysis of the methyl group has not been attempted because of the lack of a suitable reference for the optical function for this group at the air/film interface.[10,51]

(44) Timmons, C. O.; Zisman, W. A. *J. Phys. Chem.* **1965**, *69*, 984–90.
(45) See, for example: Adamson, A. W. In *Physical Chemistry of Surfaces*, 4th ed.; John Wiley: New York, 1982; p 344–8 and references therein.
(46) Hautman, J.; Klein, M. L. *J. Chem. Phys.* **1989**, *91*, 4994–5001.
(47) Harris, J.; Rice, S. A. *J. Chem. Phys.* **1988**, *89*, 5898–5908.
(48) Chau, L. K.; Porter, M. D. Unpublished results.
(49) Snyder, R. G.; Strauss, H. L.; Elliger, C. A. *J. Phys. Chem.* **1982**, *86*, 5145–50.
(50) Snyder, R. G.; Hsu, S. L.; Krimm, S. *Spectrochim. Acta, Part A* **1978**, *34*, 395–406.
(51) Stole, S. M.; Porter, M. D. *Langmuir* **1990**, *6*, 1199–1202.

Table I. C–H Stretching Mode Peak Positions[a] (cm^{-1}) for *n*-Alkanethiolate Monolayers Adsorbed at Ag, for Pure *n*-Alkanethiols, and Transition Dipole Orientations for All-Trans Alkyl Chains

n	$\nu_a(CH_3$, ip)	$\nu_a(CH_3$, op)[b,c]	$\nu_s(CH_3$, FR_1)	$\nu_a(CH_2)$[c]	$\nu_s(CH_3$, FR_2)	$\nu_s(CH_2)$
3	2963		2934		2877	
4	2964		2935		2877	
5	2965		2935		2877	
6	2964		2936		2877	
7	2964		2936		2878	
8	2964		2936		2878	
9	2964		2936		2878	
10	2964		2936		2878	2850
11	2964		2937		2878	2851
12	2964		2937		2878	2850
13	2964		2937		2878	2849
14	2964		2936		2877	2850
15	2964		2935	2919	2878	2851
17	2964		2935	2918	2878	2850
$CH_3(CH_2)_5SH$[d]	...[e]	2956		2925		2856
$CH_3(CH_2)_{11}SH$[d]	...[e]	2954		2922		2852
$CH_3(CH_2)_{17}SH$[d]	...[e]	2955		2919		2850
direction of transition dipole[f]	⊥ to C–CH_2 bond in C–C–C chain plane	⊥ to C–CH_3 bond ⊥ to C–C–C chain plane	∥ to C–CH_3 bond	⊥ to C–C–C chain plane	∥ to C–CH_3 bond	∥ to C–C–C plane, bisecting H–C–H

[a] The peak positions tabulated are obtained from three sets of samples prepared within a 24-h time period. The $\nu_a(CH_3$, ip), $\nu_s(CH_3$, FR_1), $\nu_s(CH_3$, FR_2), and $\nu_s(CH_2)$ positions are accurate to within 2 cm^{-1}. The $\nu_a(CH_2)$ peak positions are only accurate to 4 cm^{-1} due to overlap with the $\nu_s(CH_3$, FR_1) band. [b] The $\nu_a(CH_3$, op) mode is not observed in our monolayer spectra. We attribute its absence to the orientation of the $\nu_a(CH_3$, op) dipole nearly parallel to the surface. [c] We could not determine a peak position for some peaks due to low absorbance or overlap with another spectral feature. [d] Peak positions for the liquid-phase thiols $CH_3(CH_2)_5SH$ and $CH_3(CH_2)_{11}SH$ were obtained using an ATR cell. The peak positions of the crystalline-phase $CH_3(CH_2)_{17}SH$ was obtained from a KBr pellet. [e] The $\nu_a(CH_3$, ip) mode was not observed in the condensed-phase spectra. [f] Orientation of transition dipoles from: Snyder, R. G. *J. Chem. Phys.* **1965**, *42*, 1744–63.

Table II. Calculated Tilt (α) and Twist (β) Angles (deg) and Calculated and Observed Frequencies (cm^{-1}) of the $\nu_a(CH_2)$ and $\nu_s(CH_2)$ Modes for Long-Chain *n*-Alkanethiols on Ag

	$\nu_a(CH_2)$		$\nu_s(CH_2)$			
n[a]	obs	calc	obs	calc	α[b]	β[b]
12		2920	2850	2852	11	48
13		2920	2849	2852	12	41
14		2920	2850	2852	12	42
15	2919	2920	2851	2852	12	45
17	2918	2920	2850	2852	15	44

[a] Tilts calculated for n = 12–14 based on absorbances at 2919 cm^{-1}. [b] Uncertainties in α and β are ±2° and ±6°, respectively. The uncertainties were determined from the differences in the observed absorbances (sample-to-sample variation) of the $\nu_a(CH_2)$ and $\nu_s(CH_2)$ modes.

Examination of the peak positions and absorbances of the methylene stretching modes provides insights into the local environment and molecular orientation of the alkyl chains. These modes are qualitative indicators of the packing of the alkyl chains,[49,50] as shown by the differences in peak positions for the crystalline-like and liquid-like bulk *n*-alkanethiols in Table II. We therefore interpret the peak positions of $\nu_s(CH_2)$ of the long-chain monolayers as indicative of crystalline-like packing of the alkyl chains. A comparable analysis for the observed peak positions for $\nu_a(CH_2)$ points to the same interpreation for n = 15 and 17. As noted earlier, such packing implies the presence of all-trans conformational sequences in these monolayers.

The inability to determine the peak positions of the methylene modes hinders an assessment of the local environment of the hydrocarbon tails in the short-chain monolayers. The plots of the absorbances of the methylene stretching modes at the peak positions of the crystalline-like chains as a function of chain length in Figure 4a, however, suggest a similarity in the structures for the short- and long-chain monolayers. The plot of the absorbances of $\nu_s(CH_2)$ can be reasonably approximated by a straight line, which *qualitatively* points to an equivalent structure of the underlying $-(CH_2)-$ spacer group of the long- and short-chain monolayers. This interpretation is based on the infrared surface selection rule, which gives rise to the preferential excitation of vibrational modes having components of the transition dipoles normal to high reflectivity substrates.[52] A comparable treatment

Scheme II

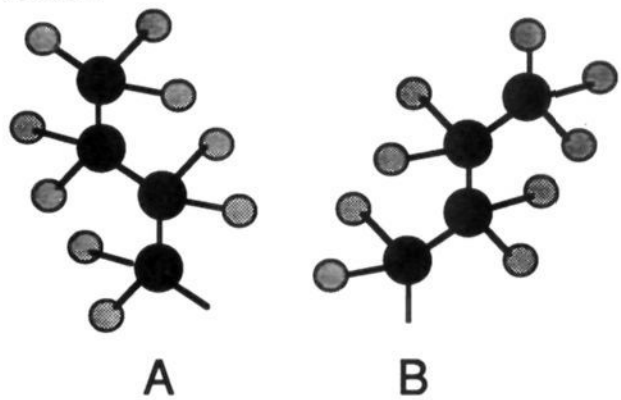

Table III. Calculated Angles[a] between the C–H Transition Dipoles and the Surface Normal for *n*-Alkanethiolate Monolayers on Ag and Au[b]

surface	α, β[c]	odd/even	$\nu_a(CH_3$, ip)	$\nu_a(CH_3$, op)	$\nu_s(CH_3)$	$\nu_a(CH_2)$	$\nu_s(CH_2)$
Ag	14, 44	odd	47 (0.47)	99 (0.02)	45 (0.50)	99 (0.02)	81 (0.02)
		even	65 (0.18)	81 (0.02)	27 (0.79)	81 (0.02)	99 (0.02)
Au	24, 50[d]	odd	72 (0.10)	72 (0.10)	26 (0.81)	72 (0.10)	105 (0.07)
		even	43 (0.53)	108 (0.10)	53 (0.36)	108 (0.10)	75 (0.07)

[a] Angles are given in degrees. The values in parentheses are the overlap parameters (see text). [b] We measure the angles between the C–H transition dipoles and the surface normal. Thus, an angle greater than 90° indicates that vector is directed toward the surface. [c] See Figure 6 for chain tilt (α) and twist (β) angle definition. [d] Data for *n*-alkanethiolates at Au are provided for comparative purposes. The α and β angles for *n*-alkanethiolates at Au determined in our laboratory are in agreement with those calculated in previous reports.[4,10]

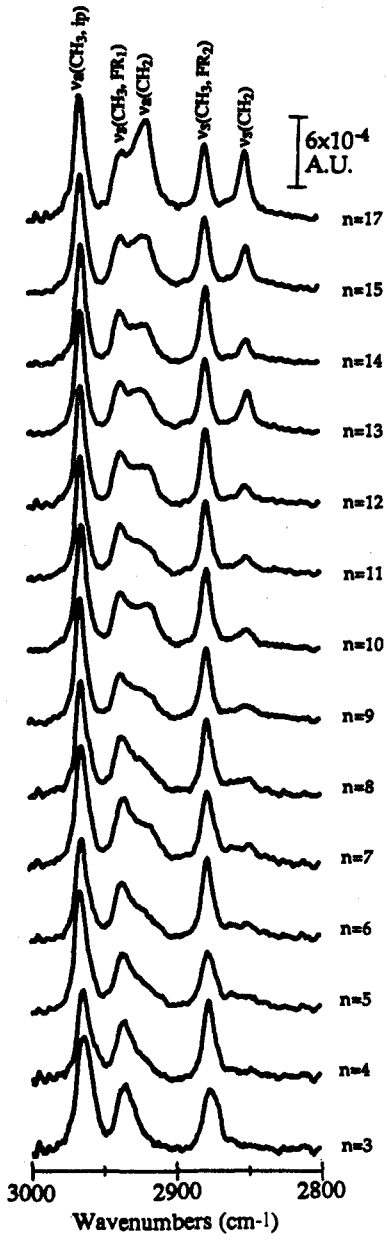

Figure 3. Infrared external reflection spectra for self-assembled monolayers of *n*-alkanethiols ($CH_3(CH_2)_nSH$) adsorbed at Ag. The p-polarized light was incident at 80°.

of the absorbances of $\nu_a(CH_2)$ is prohibited by overlap with $\nu_s(CH_3,FR_1)$.

We also carefully examined the spectral region between 1600 and 1000 cm^{-1}. Both the weak symmetric methyl deformation, $\delta(CH_3)$, and the weak methylene scissors, $\delta(CH_2)$, modes were observed, although the noise levels were such that definitive peak positions could not be determined. The noise levels also precluded the detection of methylene twist and wagging modes, which are indicative of all-trans methylene segments.[50] We also note that we have found no evidence of a highly oxidized sulfur moiety, consistent with earlier studies of "thiols at silver" by surface-enhanced Raman spectroscopy.[18,19,53]

The methylene modes also yield information about the molecular orientation of these monolayers based on the infrared surface selection rule, with average tilts between transition dipole moments (m) and the surface normal (z) calculated from[40,54]

$$\cos^2 \theta_{mz} = A_{obs}/3(A_{calc}) \quad (1)$$

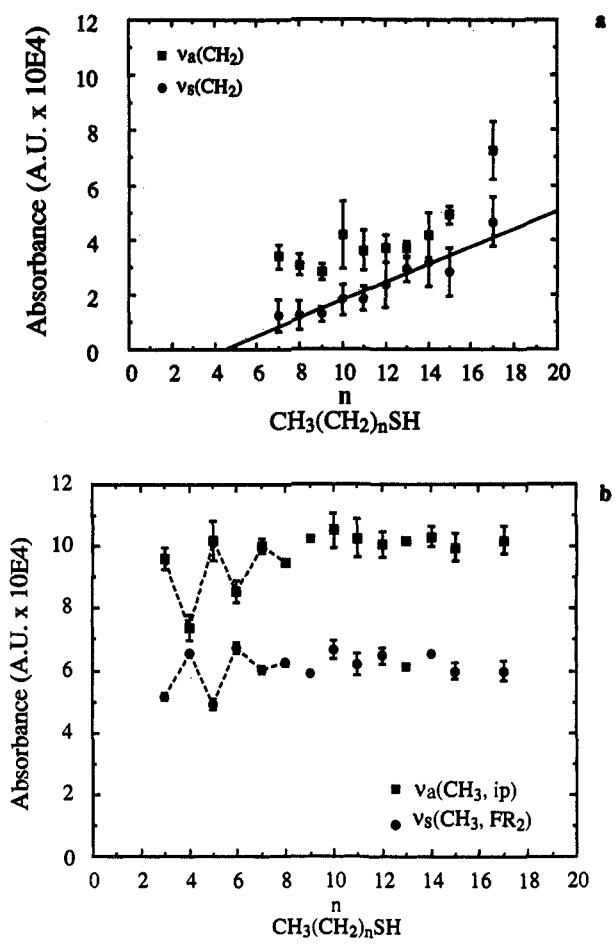

Figure 4. IR absorbances for monolayers of *n*-alkanethiols ($CH_3(CH_2)_nSH$) at Ag: (a) absorbances for the $\nu_a(CH_2)$ (■) and $\nu_s(CH_2)$ (●) bands; (b) absorbances for the $\nu_a(CH_3)$ (■) and $\nu_s(CH_3,FR_2)$ (●) modes. The error bars are the standard deviation of three samples.

where θ_{mz} is the angle of average tilt of a vibrational mode with respect to the surface normal, A_{obs} is observed absorbance, and A_{calc} is the absorbance calculated for an isotropic collection of the adsorbate precursors with comparable packing density. Thus, by relating the molecular axis of an alkyl chain (see Table I) to the transition dipole, the spatial orientation of a monolayer can be determined. It is important to note, however, that the calculated spectra for the long-chain monolayers are based on the optical function of *n*-octadecanethiol, which was determined from a Kramers–Kronig analysis of the IR spectra of the crystalline solid dispersed in KBr. This is the *reference state* for the calculations. Though not yet fully addressed from a quantitation perspective, strong perturbations in the force constants and transition dipoles of vibrational modes as a result of interactions with the substrate are not accounted for with this orientational analysis; thus, similarity of the observed and calculated peak positions and band shapes is a requisite for its implementation.[40]

Figure 5 shows the observed and calculated spectra of our *n*-octadecanethiolate monolayer at Ag, providing an example of the data for the orientational analysis. The results of the orientation calculations for this and other long-chain monolayers are shown in Table II, which summarizes of the observed and calculated peak positions of the methylene modes, the tilt angle (α) and twist angle (β). The tilt and twist angles are defined in Figure 6. The orientation analysis indicates that the $-(CH_2)-$ spacer group of our long-chain *n*-alkanethiolate monolayers at Ag exhibit respective average α's and β's of $\sim 13 \pm 2°$ and $44 \pm 6°$ (Table II). The α's also suggest a subtle increase in tilt as n increases; such changes are, however, well within the uncertainties of the

(52) Greenler, R. G. *J. Chem. Phys.* **1966**, *44*, 310–15.
(53) Bryant, M. A.; Pemberton, J. E. *J. Am. Chem. Soc.* Accepted.

(54) Wilson, E. B., Jr.; Decius, J. C.; Cross, P. C. *Molecular Vibrations*; McGraw-Hill: New York, 1955; pp 285–6.

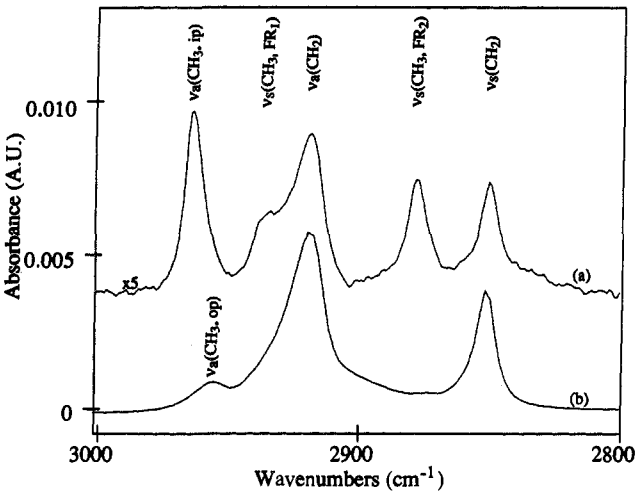

Figure 5. (a) Infrared reflection spectrum for an *n*-octadecanethiolate monolayer at Ag. (b) Calculated spectrum of a 29 Å isotropic film of *n*-octadecanethiol.

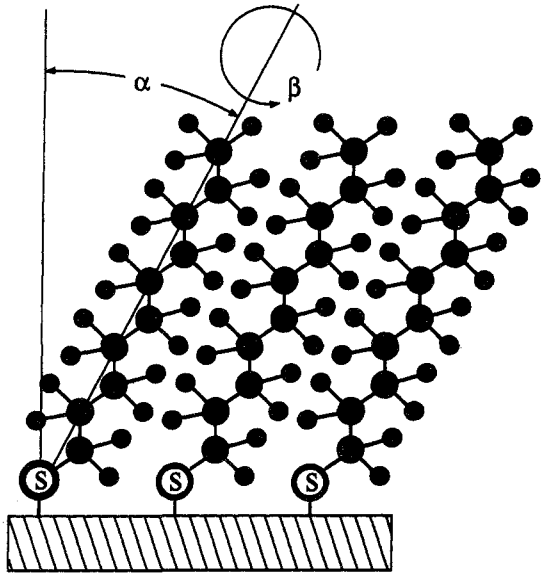

Figure 6. The tilt angle α and twist angle β of an all-trans *n*-alkanethiolate molecule adsorbed at Ag. See Table I for a description of the directions of the transition dipoles of the methyl and methylene modes.

methylene mode absorbances in Figure 4a. By inference through Figure 4a, the short-chain monolayers appear to be of analogous structure with the long-chain monolayers. We also note that the calculated and observed spectra in Figure 5 exhibit comparable peak positions and line shapes for the methylene modes. Such comparability suggests a similar distribution of the intermolecular environments for the CH_2 groups in both the reference crystalline and monolayer phases. This further supports the earlier conclusion regarding crystalline components in the structure of these monolayers.

Interestingly, the tilts of these chains differ from those for *n*-alkanethiolate monolayers at Au, and point to striking differences in the nature of both the bonding and packing densities of the monolayers at Ag. Before examining possible factors that induce such differences, we will first briefly examine possible insights into the monolayer structure from the methyl vibrational modes.

(iii) Methyl Modes. Insights concerning the orientation near the chain terminus of these monolayers are obtained from methyl stretching modes. The shape and peak positions of the asymmetric methyl stretch (see Figures 3 and 5 and Table II) indicate a predominant contribution from the in-plane mode ($\nu_a(CH_3,ip)$). Thus, in consideration of the surface selection rule and the orthogonality of the $\nu_a(CH_3,ip)$ and $\nu_a(CH_3,op)$ transition dipoles, the $\nu_a(CH_3,op)$ dipole must be oriented near the surface parallel. Such an observation is *qualitatively but not quantitatively* consistent with the calculated orientation of the underlying $-(CH_2)-$ spacer group for the long-chain monolayers which, on extension to the methyl group, yields an "overlap parameter" for $n = 17$ for the $\nu_a(CH_3,ip)$, $\nu_a(CH_3,op)$, and $\nu_s(CH_3,FR_2)$ modes of ~0.47, 0.02, and 0.50 (see Table III). We define the overlap parameter simply as $\cos^2\theta_{mz}$, which reflects the interaction of a unit transition dipole with the electric field normal to a metal surface. As such, a larger overlap parameter indicates that a unit transition dipole is aligned more with the incident electric field. With the orientation of these monolayers, the $\nu_a(CH_3,op)$ dipole has an exceedingly small perpendicular component.

The peak positions of the three methyl modes, $\nu_a(CH_3,ip)$, $\nu_s(CH_3,FR_1)$, and $\nu_s(CH_3,FR_2)$, are largely independent of chain length (Table II). However, the absorbances of the methyl modes (Figure 4b) for the short chains exhibit an odd–even dependence on the number of methylene groups in the chain, a dependence we also observe in the contact angle data for HD in Figure 2. Interestingly, this dependence is tractable only for the short-chain monolayers, a trend that we and others[53] have observed with reasonable consistency for thiolates on Ag but do not understand.

The spectroscopic origin of this odd–even progression can be understood by examining the difference in the spatial orientation of the CH_3 stretching modes for all-trans even and odd chains. Scheme II depicts two projections of ends of an *n*-alkanethiol structure with a chain orientation somewhat exaggerated from that predicted by the analysis summarized in Table II; the projections differ, however, only by a change in the sign of α. The infrared reflection spectrum in each case would exhibit a spectral pattern unique to the sign of α, which would be indicative of the orientation of the methyl group with respect to the surface normal. In moving from structure A to B, it is clear that the transition dipole for $\nu_a(CH_3,ip)$ shifts more to the surface normal, whereas that for $\nu_s(CH_3)$ shifts away from the surface normal. Thus, the absorbance for $\nu_a(CH_3,ip)$ will be greater for structure B relative to structure A, and that for $\nu_s(CH_2,FR_2)$ greater for structure A relative to B. The exaggeration of the tilt angle in Scheme II is used simply for visual purposes; the same arguments can be made for chains oriented as described in Table II.

The above spectral patterns emerge as an odd–even effect for our short-chain *n*-alkanethiolate monolayers at Ag, as shown in Figure 4b. For the odd chains ($n = 3$, 5, and 7), the absorbances for $\nu_a(CH_3,ip)$ are greater than those for the even chains ($n = 4$, 6, and 8). The pattern is reversed for the chain length dependence of the absorbance of $\nu_s(CH_3,FR_2)$. Together, these observations are consistent with the patterns predicted for structure A as an even chain and structure B as an odd chain.

A particularly meaningful observation about the odd–even effect for our monolayers at Ag is the offset by one methylene group in comparison to that at Au. *n*-Alkanethiolate monolayers at Au exhibit higher θ_a's for HD[9] and $\nu_a(CH_3,ip)$ absorbances[10] for odd-chain monolayers. Examination of molecular models reveals that only the bonding between the sulfur head group and metal substrate can reasonably account for this difference. The tilt and twist of the chains at Au[4,10] can be readily described within the framework of conventional bond angles (e.g., Au–S–C_1 bond angle ~110°;[33] see Figure 7b). A more linear Ag–S–C_1 bond angle is needed to account for the observed odd–even effect for the monolayers at Ag (see Figure 7a).

In concluding this section, we note that the above discussions present several common characteristics of the structure of the underlying $-(CH_2)-$ spacer group of our monolayers and point to a difference in the bonding of the thiol group at Ag relative to Au. However, detailing the structure at the chain terminus remains problematic. In particular, issues relating to factors that perturb the dielectric function of the end group need to be resolved. Such perturbations may arise from simple dielectric effects because of the unique local environment near the chain terminus.[10,34]

D. Structure of *n*-Alkanethiolate Monolayers at Ag and Au Surfaces. Comparing our data for *n*-alkanethiolate monolayers on Ag with that for Au[4,9,10,12] reveals two striking structural differences: tilt angle and head group binding. These differences

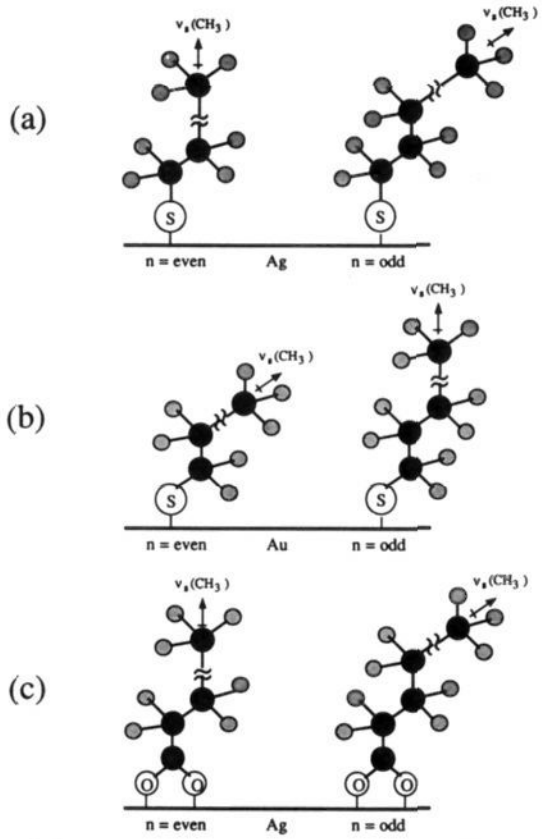

Figure 7. Proposed model for the interaction of *n*-alkanethiolate monolayers on Ag and Au surfaces accounting for the shift in the odd–even progression. The proposed structures for (a) the tilted domain of a thiolate monolayer on Ag, (b) a thiolate monolayer on Au, and (c) a carboxylate monolayer on Ag[64] for chains with an even (right) or odd (left) number of methylene groups.

must be due to dissimilarities between the Ag and Au substrates. Although the lattice mismatch between Ag and Au is only 0.3%,[55] the predominant crystal face on our evaporated Ag and Au surfaces differs. Evaporated Au films are composed largely of Au(111) crystallites.[56] Our Ag films, on the other hand, are a combination of Ag(100) and Ag(111) and/or Ag(110) domains, as evidenced by the current–potential curves for the underpotential deposition of Tl(I).[21] First, we will consider the source of the smaller tilt angle on Ag; then we will discuss a possible head group bonding model.

Based on spatial constraints, *n*-alkanethiolates can adopt different packing arrangements on each of the Ag or Au low-index planes. For example, the (100) surface can accommodate a closely packed array of interlocked alkyl chains[57] spaced 4.1 Å apart, whereas the most densely packed structures on both the (111) and (110) faces result in interchain distances of 5.0 Å. Owing to the finite size of the chains, molecules spaced 4.1 Å will be closely packed and, therefore, perpendicular to the surface. Consideration of the cohesive energy of interchain interactions predicts chains spaced 5.0 Å will be tilted ~32°.[57] A chain tilt of ~13° on (100) terraces over an extended area is therefore inconsistent with our evidence for a densely packed surface phase. We suggest that a two-domain model may explain our chain tilts: one domain with the chains perpendicular to the surface [(100) regions] and one domain with chains tilted off normal [(111) and/or (110) regions]. Thus, the calculated tilt would be a "weighted average" of two domains. Unfortunately, the overlap of the voltammetric curves for the underpotential deposition of Tl(I) permits only a rough estimation of the relative populations of the regions associated with the three low-index planes.[58] The predicted "average" tilt angle based on the relative proportions of the perpendicular and tilted portions estimated from our UPD measurements, i.e., 50% (100) and 50% (111)/(110), is ~20°. We presently attribute the discrepancy between this tilt angle and that measured experimentally (13°) to the difficulties in assessing accurately the relative populations of the different low-index planes from the UPD data. Interestingly, our preliminary STM images of these monolayers suggest the presence of a $(\sqrt{2} \times \sqrt{2})R45°$ overlayer structure (assuming a (100) arrangement of the underlying Ag) for thiols at Ag, which yields a chain packing of ~4.1 Å.[36] Although we have not as yet observed an image indicative of an overlayer at Ag(111) or Ag(110), this observation is partially supportive of the above model.

It is important to note the predominantly (111) exposed face on Au directs a ~30° chain tilt for *n*-alkanethiolate monolayers[4,10] and, as a consequence, a larger differential absorbance of CH_3 groups between even and odd chains relative to monolayers on Ag. If the Ag surfaces are composed of two domains [(100) and (111) and/or (110)], the odd–even effect arises solely from the overlayer structure at Ag(111) and/or (110).

The second distinction between the structure of *n*-alkanethiolates on Ag and on Au is an apparent difference in the head group binding. Plausible geometries of the sulfur–metal (S–M) bond along with the resulting orientations of the alkyl chains are illustrated in Figure 7a for Ag and Figure 7b for Au. The tilt of the chains in Figure 7a correspond only to that expected for these monolayers at Ag(111) or Ag(110) (i.e., the domains where the chains are tilted from the surface normal). The large (~180°) angle for the Ag–S–C_1 bond follows from the observed odd–even effect: even chains have higher $\nu_s(CH_3,FR_2)$ absorbances than odd chains. Such a bonding description is consistent with a recent study of methanethiolate at Ag(111) by sum-frequency generation spectroscopy, in which only the symmetric methyl stretch was observed.[59] We also note that the odd–even effect for *n*-alkanoic acid monolayers at Ag is qualitatively commensurate with that of the thiols on Ag; in this case, IRS provides evidence for a symmetrically bound carboxylate head group, consistent with the chain structure in Figure 7c.[60] A conventional ~110° Au–S–C_1 bond angle,[10] as shown in Figure 7b, predicts the odd–even effect for thiols at Au; even chains have higher $\nu_s(CH_3,FR_2)$ absorbances than odd chains.

Although we do not fully understand the details of the modes of bonding, it is clear that the differences in the electron-accepting ability of the two metals play an important role. There are several pieces of evidence indicating that Ag surfaces are more easily oxidized than Au surfaces, including work functions,[33] ionization potentials,[33] electronegativities,[61] and electronic band structures.[62] Since Ag is a stronger Lewis acid than Au, the bonding of thiols at Ag will be more ionic in nature; thus attachment to Ag will be more dependent on bonding through the lone pairs of electrons of sulfur. Using this reasoning, coupled with the arguments of Bond,[63] the bonding geometries in Figure 7, a and b, can be rationalized.

The above model qualitatively describes the different tilt angles observed for *n*-alkanethiolate monolayers at Ag and Au. More sophisticated descriptions of the head group bonding require molecular orbital calculations, such as those currently being explored by Hoffmann.[64] Studies underway in our laboratory involving single-crystal substrates may help to clarify the importance of the substrate crystallography in the head group bonding. We are particularly interested in testing the validity

(55) Kittel, C. *Introduction to Solid State Physics*, 5th ed.; John Wiley: New York, 1976.
(56) Reichelt, K.; Lutz, H. O. *J. Cryst. Growth* **1971**, *10*, 103–7.
(57) Ulman, A.; Eilers, J. E.; Tillman, N. *Langmuir* **1989**, *5*, 1147–52.
(58) Bewick, A.; Thomas, B. *J. Electroanal. Chem.* **1975**, *65*, 911–31.
(59) Harris, A. L.; Rothberg, L.; Dubois, L. H.; Levinos, N. J.; Dhar, L. *Phys. Rev. Lett.* **1990**, *64*, 2086–89.
(60) Schlotter, N. E.; Porter, M. D.; Bright, T. B.; Allara, D. L. *Chem. Phys. Lett.* **1986**, *132*, 93–98.
(61) Mortimer, C. E. *Chemistry A Conceptual Approach*, 4th ed.; Van Nostrand: New York, 1979; p 94.
(62) Kevan, S. D.; Gaylord, R. H. *Phys. Rev. B* **1987**, *36*, 5809–18.
(63) Bond, G. C. *Discuss. Faraday Soc.* **1966**, *41*, 200–14.
(64) Hoffmann, R. *Solids and Surfaces: A Chemist's View of Bonding in Extended Structures*; VCH Publishers: New York, 1988.

of the proposed two-domain model for our thiols on Ag.

Conclusions

We have reported a multitechnique study of *n*-alkanethiolate monolayers at evaporated Ag surfaces. Optical ellipsometry yields thicknesses which are consistent with the formation of films one molecular layer thick. Contact angle measurements of long-chain ($n \geq 12$) monolayers indicate densely packed and well-ordered films. Infrared spectroscopy shows the long-chain structures are tilted with the alkyl chains $\sim 13°$ from the surface normal, in contrast to similar structures at Au, which are tilted $\sim 30°$. Results from all three characterization methods, although less clearly defined, also indicate a comparable tilt for the shorter chain monolayers. The odd-even effect, observed in contact angle measurements and IRS, is offset by one methylene group relative to monolayers on Au. Both these differences in the structure of *n*-alkanethiolate monolayers on Ag and Au point to a difference in the bonding between the head group and the metal. Differences in the substrate crystallography and the electronic properties of the two metals provide a tractable model for the observed differences.

Together, the above results suggest the utility of "thiols on Ag" as models for fundamental studies of complex interfacial processes. In comparison to "thiols on Au", the films at Ag are more densely packed and, as we will show in forthcoming reports, more resistant to ion transport. The latter property is of particular interest to our exploration of such monolayers as applied to the surface modification of electrodes. As a result of the more reactive nature of Ag, however, the reproducible preparation of thiol monolayers is more difficult than at Au. The factors relevant to the formation of these monolayers are under study.

Acknowledgment. M.D.P. gratefully acknowledges the support of a Dow Corning Assistant Professorship. Acknowledgment is also made to the donors of the Petroleum Research Fund, administered by the American Chemical Society. We thank Dr. A. J. Bevolo for the Auger measurements. Ames Laboratory is operated for the U.S. Department of Energy by Iowa State University under Contract No. W-7405-eng-82. This work was supported by the Office of Basic Energy Sciences, Chemical Science Division.

Registry No. Ag, 7440-22-4; $CH_3(CH_2)_3SH$, 109-79-5; $CH_3(CH_2)_4SH$, 110-66-7; $CH_3(CH_2)_5SH$, 111-31-9; $CH_3(CH_2)_6SH$, 1639-09-4; $CH_3(CH_2)_7SH$, 111-88-6; $CH_3(CH_2)_8SH$, 1455-21-6; $CH_3(CH_2)_9SH$, 143-10-2; $CH_3(CH_2)_{10}SH$, 5332-52-5; $CH_3(CH_2)_{11}SH$, 112-55-0; $CH_3(CH_2)_{12}SH$, 19484-26-5; $CH_3(CH_2)_{13}SH$, 2079-95-0; $CH_3(CH_2)_{14}SH$, 25276-70-4; $CH_3(CH_2)_{15}SH$, 2917-26-2; $CH_3(CH_2)_{17}SH$, 2885-00-9; hexadecane, 544-76-3.

Upper Rim Calixcrowns: Elucidation of the Mechanism of Conformational Interconversion of Calix[4]arenes by Quantitative 2-D EXSY NMR Spectroscopy

Jan-Dirk van Loon,[†] Leo C. Groenen,[†] Sybren S. Wijmenga,[‡] Willem Verboom,[†] and David N. Reinhoudt*[,†]

Contribution from the Department of Organic Chemistry, University of Twente, 7500 AE Enschede, The Netherlands, and the National HF-NMR Facility, University of Nijmegen, 6525 ED Nijmegen, The Netherlands. *Received July 27, 1990*

Abstract: Tetramethoxycalix[4]arenes (**4-8**) bridged by a polyether chain at the *upper rim* (upper rim calixcrowns) were synthesized by reaction of 5,17-bis(chloromethyl)-25,26,27,28-tetramethoxycalix[4]arene (**3**) with poly(oxyethylene) glycols of different length (mono to penta). In $CDCl_3$ solution at −20 °C, these compounds exist as a mixture of *two conformations*, viz. the partial cone (P) and the cone (C). The P/C ratio varies between 4.0 and 1.7 depending on the length of the bridge. The upper rim calixcrowns are flexible molecules according to temperature-dependent ^1H NMR spectroscopy. *For the first time* the mechanism of conformational interconversion of calix[4]arenes (**4** and **5**) was elucidated by quantitative 2-D EXSY NMR spectroscopy. It proves that there are *two different pathways* (a slow and a fast process) by which the two P conformational topomers can interconvert. One interconversion proceeds via C (slow process), and the other process proceeds most likely via a short-lived 1,3-alternate (A) intermediate (fast process). The rate constants for both pathways were determined; calix[4]crown-2 **4**, $k_{PA} = 0.58$, $k_{PC} = 0.054$, and $k_{CP} = 0.27$ s^{-1} at 298 K, and calix[4]crown-3 **5**, $k_{PA} = 5.4$, $k_{PC} = 0.07$, and $k_{CP} = 0.18$ s^{-1} at 253 K. The overall rate diminishes dramatically going from a nine-atom bridge in **5** to a six-atom bridge in **4**. Furthermore, shortening of the bridge has a much larger decelerating effect on the P → A than on the P → C process.

Introduction

The rational design of specific receptors for the selective binding of (neutral) guests is a rapidly growing field of interest in supramolecular chemistry.[1,2] Therefore, it is important to develop three-dimensional building blocks for the attachment of functional groups that can be oriented in space in such a way that they can form a suitable binding site. In particular, calix[4]arene **1** (Chart I), a cyclic tetramer composed of phenolic units which are linked via the ortho positions by methylene bridges,[3] is recognized to be such an important molecular building block. Calix[4]arene is readily available from cheap starting materials,[4] and it can be easily functionalized at the phenolic OH groups (lower rim)[3] as well as at the para positions of the phenol rings (upper rim).[3,5]

[†] University of Twente.
[‡] University of Nijmegen.

(1) (a) Lehn, J.-M. *Angew. Chem.* **1988**, *100*, 91-119. (b) Cram, D. J. *Angew. Chem.* **1988**, *100*, 1041-1052. (c) Diederich, F. *Angew. Chem.* **1988**, *100*, 372-396. (d) Collet, A. *Tetrahedron* **1987**, *43*, 5725-5759. (e) Koga, K.; Odashima, K. *J. Inclusion Phenom. Mol. Recognit. Chem.* **1989**, *7*, 53-60. (f) Reinhoudt, D. N.; den Hertog, Jr., H. J. *Bull. Soc. Chim. Belg.* **1988**, *97*, 645-653. (g) Reinhoudt, D. N.; Dijkstra, P. J. *Pure Appl. Chem.* **1988**, *60*, 477-482.

(2) (a) Weber, E. *Progress in Macrocyclic Chemistry* (*Synthesis of Macrocycles, the Design of Selective Complexing Agents*); Izatt, R. M., Christensen, J. J., Eds.; John Wiley & Sons: New York, 1989; Vol. 3, pp 337-419. (b) Hamilton, A. D.; Muehldorf, A.; Chang, S.-K.; Pant, N.; Goswami, S.; van Engen, D. *J. Inclusion Phenom. Mol. Recognit. Chem.* **1989**, *7*, 27-38. (c) Rebek, Jr., J. *Angew. Chem., Int. Ed. Engl.* **1990**, *29*, 245-255. (d) Zimmerman, S. C.; Wu, W. *J. Am. Chem. Soc.* **1989**, *111*, 8054-8055.

0002-7863/91/1513-2378$02.50/0